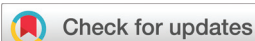


PAPER

Cite this: *Nanoscale*, 2023, 15, 13699

Ultralow reaction barriers for CO oxidation in Cu–Au nanoclusters†

 Anastasiia A. Mikhailova,^a Sergey V. Lepeshkin,^{a,b,c} Vladimir S. Baturin,^a Alexey P. Maltsev,^a Yurii A. Uspenskii^b and Artem R. Oganov^a

Systematic structure prediction of Cu_nAu_m nanoclusters was carried out for a wide compositional area ($n + m \leq 15$) using the evolutionary algorithm USPEX and DFT calculations. The obtained structural data allowed us to assess the local stability of clusters and their suitability for catalysis of CO oxidation. Using these two criteria, we selected several most promising clusters for an accurate study of their catalytic properties. The adsorption energies of reagents, reaction paths, and activation energies were calculated. We found several cases with low activation energies and explained these cases using the patterns of structural change at the moment of CO_2 desorption. The unique case is the Cu_7Au_6 cluster, which has extremely low activation energies for all transition states (below 0.05 eV). We thus showed that higher flexibility due to the binary nature of nanoclusters makes it possible to achieve the maximum catalytic activity. Considering the lower price of copper, Cu–Au nanoparticles are a promising new family of catalysts.

Received 3rd May 2023,
Accepted 22nd July 2023
DOI: 10.1039/d3nr02044d
rsc.li/nanoscale

1. Introduction

Nanoclusters containing 10–1000 atoms have unique optical, magnetic, chemical, and other properties not observed in the corresponding bulk materials and are therefore subject of active research. The properties of nanoclusters, especially smaller-sized ones, strongly depend on the number of atoms in the cluster. This is especially important for catalytic properties: the smaller the size of catalytic particles, the larger the specific surface area of a catalyst.

The first experimental investigations performed with small Au nanoparticles supported by metal oxides (TiO_2 , Fe_2O_3 , etc.) have shown that they have prominent catalytic activity for many reactions, in particular, for CO oxidation.^{1–6} At room temperature and lower temperatures, they are often superior to classical catalysts such as Pt and Pd. Despite many subsequent studies (see reviews^{7–9}), the mechanisms causing this remarkable enhancement remain poorly understood. Important information about reaction features can be obtained from first-principles calculations.^{10–12}

Gao *et al.* have studied the catalytic activity and active center locations in gold clusters Au_n ($n \leq 35$).¹³ It has been shown that the maximum binding energy is observed at sites with reduced coordination number or with a small angle of the cone formed by adjacent bonds. A correlation has also been found between catalytic activity, adsorption energy, and structural properties through the Sabatier principle and the Brønsted–Evans–Polanyi relationship; the catalytic activity can be well characterized by rather simple structural descriptors.^{14–16} Another way to assess adsorption, and hence catalytic properties, is to study the electronic structure.^{17,18} An increase in the catalytic activity of gold nanoclusters has been observed as the d-band narrows and shifts to the Fermi level. Gold has excellent catalytic properties and long lifespan¹⁹ but is expensive; therefore, finding a cheaper material with similar properties is highly desirable.

Copper catalysts are a well-studied class of materials that have comparable catalytic activity and relatively low priced. Copper is used in a wide range of chemical reactions, including the oxidation of CO.^{8,20–22} The principal limitation of its

^aSkolkovo Institute of Science and Technology, Bolshoy Boulevard 30, bld. 1, 121205 Moscow, Russian Federation. E-mail: Anastasiia.Mikhailova@skoltech.ru

^bLebedev Physical Institute, Russian Academy of Sciences, 53 Lenin Avenue, 119991 Moscow, Russian Federation

^cVernadsky Institute of Geochemistry and Analytical Chemistry Russian Academy of Sciences, 19 Kosygin St, 119991 Moscow, Russian Federation

†Electronic supplementary information (ESI) available: Fig. S1: ground-state structures of Cu_nAu_m clusters ($n + m \leq 15$). Fig. S2: density of electronic states—total (black line) and projected on d-orbitals (red fill) in 6 characteristic clusters: Cu_6 (planar), Cu_{12} (non-planar), Cu_{14} (non-planar), Au_6 (planar), Au_{12} (planar), and Au_{14} (non-planar). Fig. S3: computed reaction pathways of $\text{CO} + \text{O}_2 \rightarrow \text{CO}_2 + \text{O}^*$ on both stable and catalytically active Cu_nAu_m clusters. Here, * denotes the species adsorbed on a cluster. Table S1: computed relative energy (eV), with respect to the reactant in the gas phase ($\text{CO} + \text{O}_2$) of the co-adsorption states, the first transition state (TS1), intermediate states ($\text{O}-\text{O}-\text{C}-\text{O}^*$), the second transition state (TS2), and the final state ($\text{CO}_2 + \text{O}^*$) for $\text{CO} + \text{O}^* \rightarrow \text{CO}_2$ during CO oxidation on the clusters that are both stable and catalytically active. N – number of the pathway. Cartesian coordinates of Cu–Au clusters in the XYZ format for which catalytic pathways were calculated. See DOI: <https://doi.org/10.1039/d3nr02044d>

use is the active oxidation of copper itself,^{20,23} which can be decreased by alloying with various elements (*i.e.* Au, Pt, Pd).^{24–27} Bimetallic or multicomponent clusters are now emerging as a substantial advancement in catalysis.¹⁸ They usually have a core–shell structure, where only the shell is formed by catalytically active metals. Such a morphology leads to significant cost reduction of a catalyst. In addition, bimetallic nanocatalysts demonstrate a synergistic effect, and are more catalytically active than those formed from pure constituent components.²⁸ Specifically, the Cu–Au system is of interest because of its high corrosion resistance,^{22,29} lower cost, and the ability to control its catalytic properties by changing its structural characteristics such as the copper-to-gold ratio.^{30–32}

Moving from one-component to bimetallic catalysts opens the door to a number of reaction mechanisms that exploit component difference. The Langmuir–Hinshelwood (LH) mechanism suggests that both reactants (CO and O₂) are adsorbed at the catalyst surface where the oxidation reaction takes place. The Eley–Rideal (ER) mechanism suggests the adsorption of only one reactant while the other one remains gaseous. The ER kinetics is close to the LH one when the latter has reactants adsorbed on different sorts of active sites and one reactant is weakly adsorbed.³³ The feature of the Mars–van Krevelen (MvK) mechanism is that one reactant is adsorbed at the catalyst surface while the other is adsorbed on the top of the first reactant. The LH mechanism has been applied to most studies related to Au nanoparticles and nanoclusters.^{13,34} At the same time, the use of the ER mechanism is limited because of the weak adsorption and dissociation of O₂ on Au. The importance of an oxide layer for the catalytic oxidation of CO has been noted by many researchers.^{4,35–37} In recent years, this observation and the high oxidation of Cu atoms have been constructively used for the fabrication of efficient Cu–Au catalysts. It was found that preliminary annealing in air or oxygen forms a CuO_x layer at the CuAu surface, which significantly enhances the CO conversion perhaps *via* the MvK mechanism.^{12,38} Reconstruction of the structure during CuO_x layer formation was examined in detail by experiments and DFT calculations,^{12,38} while the process of CO oxidation itself is still not well understood as catalyst complexity makes many pathways of the reaction possible. When preliminary annealing is absent, the structure of a CuAu catalyst is not so complicated and the CO conversion is most likely to follow the LH mechanism.

Previous theoretical studies on the rationalization of catalytic nanoparticles give many important insights into how catalytic properties may be assessed from other characteristics. However, they are focused mostly on model particles with intuitively constructed structures. These studies either considered very small clusters predicted using accurate and computationally demanding methods or used semiempirical approaches for larger particles, with parameters derived from bulk species. For copper–gold nanoclusters, little to no attention has been paid to thorough investigation of reaction pathways—the most comprehensive characteristic of catalytic activity. In this work, we provide an extensive systematic

picture of Cu–Au bimetallic nanoparticles with up to 15 atoms, including their equilibrium structures and stability. On the basis of well-known descriptors, we select particles that are both stable and promising for CO oxidation, study them using an accurate *ab initio* analysis of the corresponding reaction pathways and show that copper–gold nanoparticles can be on a par with or even superior to gold nanoparticles in catalytic activity, while being significantly cheaper.

2. Computational methods

The ground-state structures of Cu_nAu_m clusters were obtained in a large compositional area using the variable composition technique³⁹ for the global optimization of nanocluster structures implemented in the evolutionary algorithm USPEX.^{40,41} This method demonstrated 5–50 times higher speed than the traditional USPEX code for each composition.^{39,42,43}

Global optimization was carried out in two steps. First, we predicted the structures using the Gupta potential⁴⁴ using the evolutionary algorithm USPEX coupled with a large-scale atomic/molecular massively parallel simulator (LAMMPS).⁴⁵ Then, 30 lowest-energy structures for each composition were used as seed structures (known structures of a specific compound for the initial generation in the evolutionary algorithm USPEX) to continue calculations in the evolutionary algorithm USPEX coupled with the VASP code within density functional theory (DFT). Our calculations are spin-polarized and used the projector augmented wave method (PAW)⁴⁶ and the Perdew–Burke–Ernzerhof (PBE)⁴⁷ generalized gradient approximation exchange correlation functional as implemented in the Vienna *ab initio* simulation package (VASP),^{48,49} where we set a plane wave energy cutoff of 295 eV and a vacuum layer of 8 Å between the periodic images of the cluster.

Selected catalytically active clusters and all further CO oxidation reactions with them were calculated using dispersion corrections (PBE@MBD)⁵⁰ with an energy cutoff of 600 eV, and the periodic images of a cluster were separated using a vacuum layer of 12 Å in the VASP code.^{48,49} We examined various positions of CO and O₂ molecule attachment for the initial and final states of the CO oxidation reaction and selected the most energetically favorable among them. The adsorption energy is defined as $E_{\text{ads}} = E(\text{adsorbate} + \text{cluster}) - E(\text{cluster}) - E(\text{adsorbate})$, where $E(\text{adsorbate} + \text{cluster})$ is the total energy of a composite cluster and an adsorbate system, $E(\text{cluster})$ is the energy of a freestanding cluster, and $E(\text{adsorbate})$ is the energy of an isolated adsorbate. The reaction barriers and pathways for CO oxidation were calculated using the nudged elastic band method (NEB)^{51,52} implemented in the VASP code. For all ground states, frequencies were calculated and $3N - 6$ positive frequencies were found (N – number of atoms). Only one significant imaginary frequency was found in each of the transition states.

3. Results and discussion

The most stable structures of all calculated Cu_nAu_m clusters ($n + m \leq 15$) are shown in ESI Fig. S1.† Some structures important for further analysis are presented in Fig. 1. Our results reproduced previous calculations for smaller clusters^{53–56} or

improved on them for Cu_2Au_8 , Cu_8Au_2 , and Cu_3Au_7 clusters. The ground-state structures of Cu_nAu_m clusters with $11 \leq n + m \leq 15$ were found for the first time.

Fig. 2a shows the compositional areas with planar and non-planar clusters. Small Cu_nAu_m clusters ($n + m \leq 6$) have only planar structures. Structures with $7 \leq n + m \leq 13$ show greater

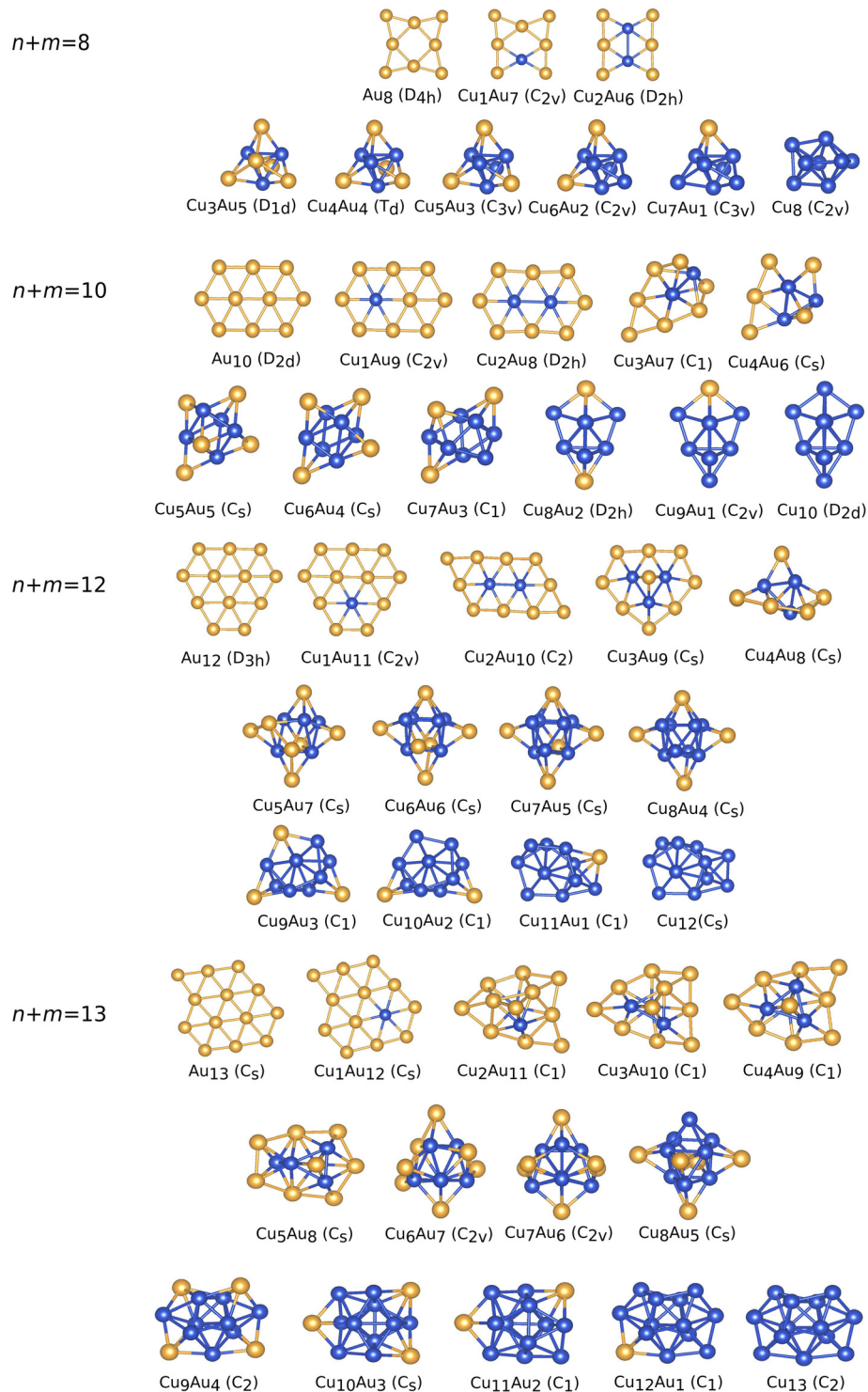


Fig. 1 Optimal structures of selected stable Cu_nAu_m clusters.

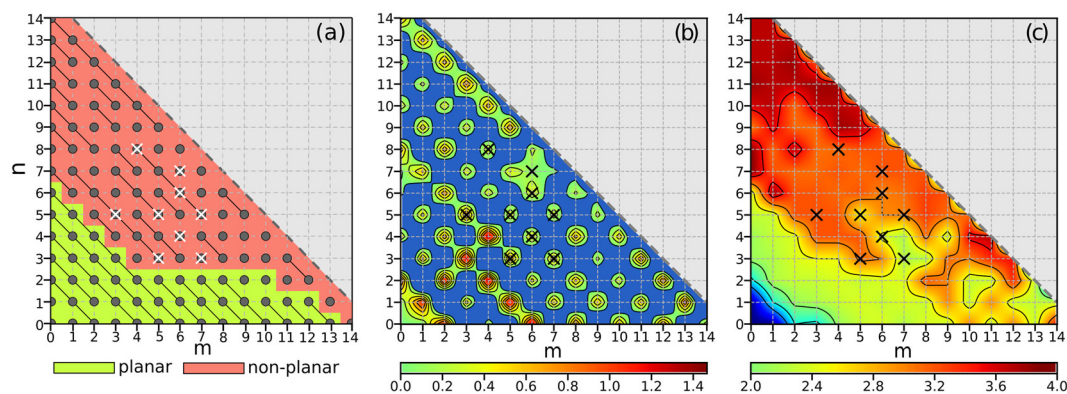


Fig. 2 Characteristics of Cu_nAu_m clusters mapped in the (n, m) coordinates: (a) compositional areas with planar and nonplanar structures, clusters with similar shapes are connected; (b) $\Delta_{\min}^2(n, m)$ in eV; (c) minimum coordination numbers $\text{CN}_{\min}(n, m)$. The clusters selected for CO oxidation are marked with crosses.

diversity: pure Au clusters and clusters with one or two copper atoms are planar, whereas higher copper concentration induces transformation to a non-planar morphology. Clusters with 14 or more atoms are most likely to be always non-planar only. Thus, Au-rich clusters tend to be planar and to have low-coordinated atoms. These tendencies are characteristic of covalent bonding and require the participation of directional p- or d-orbitals, rather than only spherical s-orbitals, such as the 6s-orbitals of Au. The closed 5d-shell of Au also has a spherical symmetry and cannot explain directionality. In our opinion, the origin of directed bond character is the s-d hybridization, which admixes d-orbitals to s-states, leading to strongly angular-dependent hybrid orbitals. This admixing is clearly seen in Fig. S2†. Near the Fermi energy the eye catches that d-contributions are much larger in gold clusters than in copper ones. Possible factors responsible for this effect are (i) a larger (about 10%) radius of Au 5d-orbitals that enhances the matrix element of s-d mixing and (ii) a deeper position of the Cu 3d-band which decreases d-state admixing (an equal energy of the band top in Cu_6 and Au_6 is a rare exception to this rule). These factors explain the different morphologies of Cu- and Au-rich clusters (Fig. 2a).

Another important structural feature of Cu-Au nanoparticles is their core-shell structure with Au atoms forming the shell. Such a morphology follows from the larger size of gold atoms than that of copper, which favors a smaller density of Au atoms on the surface. This agrees with the difference in the surface energies of pure copper and gold (2.03 and 0.93 J m^{-2} correspondingly), which has been experimentally observed by Chmielewski *et al.*⁵⁷ for Cu-Au nanoparticles.

We also note that the shape of a cluster often remains the same when an atom of gold is replaced by copper or *vice versa*. This is observed, *e.g.*, in $\text{Cu}_{3+x}\text{Au}_{5-x}$ series, $x = 1-3$ (Fig. 1). To reflect this behavior, we connected the clusters of the same shape with solid lines in Fig. 2a.

Because of the limitations of available experimental techniques, the synthesized nanoparticles usually show a size distribution. In addition, it is important to investigate stability in

a wide range of compositions. Criteria of thermodynamic stability are not applicable to nanoparticles; therefore, we used the criteria of local, or conditional, stability. We took the second-order finite differences of the total energy with respect to the number of atoms and found their minimum:

$$\Delta_{\min}^2(n, m) = \min\{\Delta_{\text{Cu}}^2(n, m), \Delta_{\text{Au}}^2(n, m)\} \quad (1)$$

where

$$\begin{aligned} \Delta_{\text{Cu}}^2(n, m) &= E(n+1, m) + E(n-1, m) - 2E(n, m) \\ \Delta_{\text{Au}}^2(n, m) &= E(n, m+1) + E(n, m-1) - 2E(n, m) \end{aligned} \quad (2)$$

and $E(n, m)$ is the ground-state energy of the Cu_nAu_m cluster. The value of $\Delta_{\min}^2(n, m)$ is the measure of stability, and if it is positive, the cluster is called “magic”. Numerically, $\Delta_{\min}^2(n, m)$ characterizes the stability of a cluster against the transfer of one atom of each type between a pair of identical Cu_nAu_m molecules. In experiments, clusters are synthesized in ensembles, and therefore this value can be a measure of the abundance of a cluster. The results demonstrate the parity effect – enhanced stability of clusters with even numbers of electrons (Fig. 2b). This indicates the tendency of the clusters to have closed shell electronic structure. One exception is the Cu_7Au_6 cluster, which is both stable and open-shell, which can be explained by its high symmetry (C_{3v}). Generally, the stability of clusters is determined by two factors: the closed-shell electronic structure and the atomic closed-shell structure.

Having identified stable clusters, we screened them for potential catalytic activity. An obvious way to do so is to calculate the reaction paths and the reaction barriers, but such calculations are extremely computationally demanding. Given the number of clusters considered here, it is highly desirable to find simple descriptors to discard the unpromising cases. One of them is the coordination number, which has been used to approximate adsorption properties and catalytic activity. In general, the following pattern is expected: underbound and low-coordinated atoms have greater catalytic activity. Previous studies have suggested that two- and three-coordinated atoms

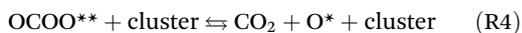
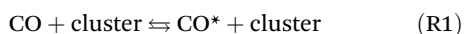
serve as catalytically active sites and promote general efficiency.^{13,14} In this study, we evaluated the coordination number of an atom as follows:

$$\text{CN}_i = \sum_j c_{ij}$$

$$c_{ij} = \begin{cases} \exp\left(-\frac{r_{ij}-R_{ss'}}{D}\right), & \text{if } r_{ij} \geq R_{ss'} \\ 1 & \text{if } r_{ij} < R_{ss'} \end{cases} \quad (3)$$

where i is the number of a given atom; r_{ij} is the distance between atoms i and j having sorts $s = s(i)$ and $s' = s'(j)$; $R_{ss'}$ is the reference length of a bond between the atoms of s and s' sorts (we took the values of 3.0 Å, 2.85 Å and 2.7 Å for Au–Au, Au–Cu and Cu–Cu pairs); and $D = 0.37$ Å is the empirically determined parameter. To illustrate the dependence of the minimum coordination number $\text{CN}_{\min} = \min\{\text{CN}_i\}$ on the cluster composition, we built an interpolated map of the minimum coordination numbers $\text{CN}_{\min}(n, m)$ for the ground-state clusters of each composition (see Fig. 2c). The coordination numbers of surface atoms in planar and non-planar structures vary from 2 to 3 and from 2 to 4, respectively. In comparison, the core atoms have coordination numbers between 3 and 9.

Using the maps of stability and minimum coordination numbers, we selected stable clusters that have low-coordinated surface atoms, marked with crosses on the maps (Fig. 2), for a more detailed consideration of catalytic properties. We calculated the reaction barriers and pathways for CO oxidation on the selected clusters, which can proceed *via* two mechanisms: the Langmuir–Hinshelwood mechanism assumes the adsorption of both CO and O₂ molecules on the nanoparticle surface,⁵⁸ whereas the Eley–Rideal mechanism⁵⁹ suggests the adsorption of only one molecule. In this work, we followed the Langmuir–Hinshelwood mechanism because the adsorption and dissociation of O₂ on Au are hindered by unfavorable kinetics.^{60,61} The mechanism consists of the following elementary reactions:



where * denotes the species adsorbed on a cluster, ** denotes the adsorption on two sites of a cluster.

For each selected cluster, we modeled the reactions with the CO molecules adsorbed on two- and three-coordinated surface atoms responsible for catalytic activity. The selected cases allowed us to consider different environments of active sites. For example, in the case of Cu₅Au₇, there are three possible scenarios: (1 and 2) CO is adsorbed on the three-coordinated Au active site, surrounded by one Au and two Cu neighbors, whereas O₂ is adsorbed on either Au or Cu neighbor; (3) CO is adsorbed on the three-coordinated Au active site, with three neighboring Cu atoms, and O₂ is adsorbed on one

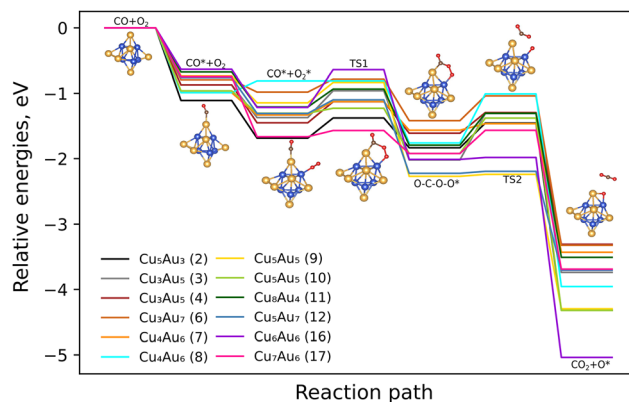


Fig. 3 Computed reaction pathways of CO + O₂ → CO₂ + O* on both stable and catalytically active Cu_nAu_m clusters. Here, * denotes the species adsorbed on a cluster.

of these Cu neighbors. The most thermodynamically and kinetically favorable pathways for each considered cluster are shown in Fig. 3. The calculated pathways for each reaction are shown in ESI Fig. S3.† The activation barriers and adsorption energies are shown in Table 1. The relative energies of intermediates are presented in ESI Tables S1.†

The reaction mechanism starts with the adsorption of CO and O₂ (stages R1 and R2 in eqn (4)). CO adsorption (R1) always proceeds without a kinetic barrier. Seventeen out of the 18 selected clusters have Au atoms as active sites. The corresponding adsorption energies E_{ad} vary from −0.63 to −1.0 eV and appear to be independent of the environments of active sites. The remaining case is the Cu₅Au₃ cluster with the three-coordinated Cu atom as an active site. It has the strongest adsorption with $E_{\text{ad}} = -1.11$ eV.

The second stage (R2), the adsorption of the oxygen molecule, usually has no kinetic barrier. The energy gain depends on whether the O₂ is adsorbed on Cu or Au atoms. The adsorption on copper is generally more favorable, with energies from −0.58 to −0.34 eV. For O₂ adsorbed on Au atoms, this range is from −0.34 to −0.08 eV, which can be explained by stronger binding to copper than to more inert gold. We note two outlying cases: Cu₇Au₆ and Cu₄Au₆. In the former one, O₂ is efficiently adsorbed on the Cu atom of the Cu₇Au₆ cluster with an energy gain of 0.92 eV. This may be related to the cluster's higher reactivity due to its open-shell electronic structure. In the Cu₄Au₆ cluster, in contrast, the adsorption energy is positive ($E_{\text{ad}} = +0.18$ eV), meaning that the unbound state is more favorable. This has been observed previously for Au_n clusters.³⁴

In the next stage (R3), the adsorbed CO* and O₂* molecules bond with each other to form an OCOO** intermediate (Fig. 3). This process goes through a transition state TS1 with the activation energy E_{a} varying from 0.05 to 0.61 eV. In most cases, it is below ~0.3 eV, which is not a significant obstacle in the catalytic pathway, and this transformation can probably proceed under mild conditions. The lowest barriers (~0.10 eV) are observed in Cu₅Au₅ and Cu₅Au₇ clusters, as well as in the Cu₇Au₆ cluster, the only stable open-shell cluster. The latter

Table 1 Calculated activation and adsorption energies for CO and O₂ in CO oxidation on clusters that are both stable and catalytically active. *N* – number of the pathway. Numbers in parentheses indicate the number of the atom in the XYZ coordinates (see the ESI†)

| <i>N</i> | Cluster | Atom for CO | <i>E</i> _{ad} (CO), eV | Atom for O ₂ | <i>E</i> _{ad} (O ₂), eV | First activation energy ^a , eV | First reaction energy, eV | Second activation energy ^a , eV | Second reaction energy, eV |
|----------|---------------------------------|--------------|---------------------------------|-------------------------|--|---|---------------------------|--|----------------------------|
| 1 | Cu ₅ Au ₃ | Au (atom 6) | -0.82 | Cu (atom 1) | -0.54 | 0.61 | -0.42 | ≈0 | -1.56 |
| 2 | Cu ₅ Au ₃ | Cu (atom 4) | -1.11 | Cu (atom 5) | -0.58 | 0.31 | -0.15 | 0.38 | -2.49 |
| 3 | Cu ₃ Au ₅ | Au (atom 4) | -0.87 | Cu (atom 3) | -0.50 | 0.41 | -0.65 | 0.71 | -1.72 |
| 4 | Cu ₃ Au ₅ | Au (atom 8) | -0.92 | Cu (atom 3) | -0.54 | 0.32 | -0.16 | 0.32 | -1.70 |
| 5 | Cu ₃ Au ₅ | Au (atom 8) | -0.92 | Au (atom 6) | -0.24 | 0.53 | -0.39 | ≈0 | -2.22 |
| 6 | Cu ₃ Au ₇ | Au (atom 8) | -0.79 | Au (atom 10) | -0.19 | 0.20 | -0.44 | 0.38 | -1.91 |
| 7 | Cu ₄ Au ₆ | Au (atom 10) | -0.99 | Cu (atom 3) | -0.34 | 0.21 | -0.23 | 0.10 | -1.87 |
| 8 | Cu ₄ Au ₆ | Au (atom 10) | -0.99 | Au (atom 8) | 0.18 | 0.18 | -0.95 | 0.75 | -2.20 |
| 9 | Cu ₅ Au ₅ | Au (atom 8) | -0.73 | Cu (atom 4) | -0.41 | 0.31 | -1.13 | ≈0 | -2.03 |
| 10 | Cu ₅ Au ₅ | Au (atom 9) | -0.96 | Cu (atom 4) | -0.34 | 0.08 | -0.62 | 0.54 | -2.40 |
| 11 | Cu ₈ Au ₄ | Au (atom 9) | -0.68 | Cu (atom 3) | -0.53 | 0.27 | -0.58 | 0.49 | -1.71 |
| 12 | Cu ₅ Au ₇ | Au (atom 6) | -0.76 | Cu (atom 2) | -0.55 | 0.21 | -0.92 | ≈0 | -1.48 |
| 13 | Cu ₅ Au ₇ | Au (atom 11) | -0.71 | Cu (atom 5) | -0.49 | 0.26 | -0.43 | 0.37 | -1.73 |
| 14 | Cu ₅ Au ₇ | Au (atom 11) | -0.71 | Au (atom 12) | -0.08 | 0.11 | -1.03 | 0.17 | -1.87 |
| 15 | Cu ₆ Au ₆ | Au (atom 11) | -0.63 | Au (atom 8) | -0.34 | 0.29 | -0.70 | 0.52 | -1.55 |
| 16 | Cu ₆ Au ₆ | Au (atom 11) | -0.63 | Cu (atom 5) | -0.58 | 0.58 | -0.80 | ≈0 | -3.03 |
| 17 | Cu ₇ Au ₆ | Au (atom 10) | -0.75 | Cu (atom 3) | -0.92 | 0.10 | -0.26 | 0.36 | -1.77 |
| 18 | Cu ₇ Au ₆ | Au (atom 10) | -0.75 | Cu (atom 5) | -0.43 | 0.05 | -0.22 | ≈0 | -1.87 |

^a In cases where a reaction involves several barriers, one has to carefully determine which barrier limits the reaction rate.⁶² In all cases studied here there are two barriers, and the highest one is the rate-limiting one.

case is consistent with previous results for Au clusters³⁴ with odd numbers of electrons.

Finally, the OCOO** complex undergoes O–O bond breaking and decomposes into an isolated CO₂ molecule and an adsorbed O* atom (stage R4). The activation energy for the corresponding transition state TS2 strongly depends on the coordination of the remaining oxygen atom at the moment of CO₂ detachment: if O* is bound to one atom (Au or Cu), then *E*_a is between 0.32 and 0.75 eV, whereas when O* is bound to

two atoms one of which is Cu, the barrier drops to extremely low values of several meV. Such a reduction of the barrier, indicating high catalytic activity, is observed in Cu₅Au₃, Cu₃Au₅, Cu₅Au₅, Cu₅Au₇, Cu₆Au₆, and Cu₇Au₆ clusters (Table 1). Typical examples of mechanisms with two different coordinations of O* at the moment of CO₂ detachment, together with corresponding energetics, are shown in Fig. 4.

In the final stage of the reaction, the adsorbed O* atom is bonded with two or three atoms of Cu and Au. The adsorption

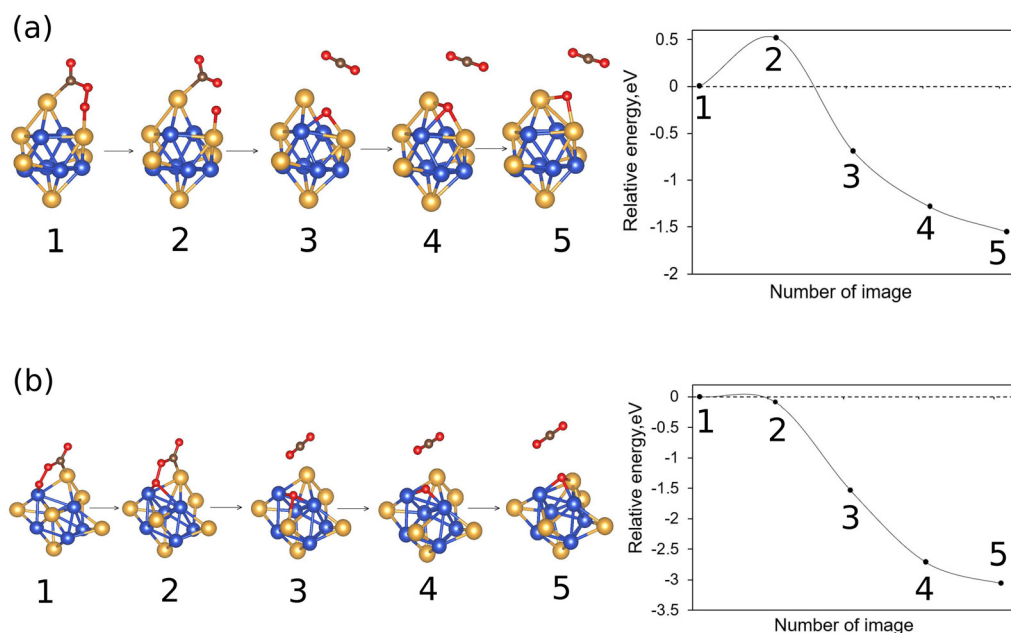


Fig. 4 Mechanisms of OCOO* decomposition: (a) with usual barriers; (b) with ultralow barriers.

energy varies from -1.6 to -2.1 eV, which is in close agreement with the results obtained by Chepkasov *et al.*³²

In the calculated potential energy surfaces, turnover frequency (TOF)-determining intermediates⁶² (the intermediates which have the lowest energy) and TOF-determining transition states⁶² (the highest TS following the rate-determining intermediate) follow immediately one after another, so the limiting stage of each pathway is the step with the highest activation barrier. The median limiting activation barrier of the whole reaction (R1–R4) is not higher than 0.4 eV and can be overcome under mild conditions. We also found special clusters with extremely low activation energies (several meV): Cu₅Au₅, Cu₅Au₇, and Cu₇Au₆ have a low first barrier; Cu₅Au₃, Cu₃Au₅, Cu₅Au₅, Cu₅Au₇, Cu₆Au₆, and Cu₇Au₆ have a low second barrier. The Cu₇Au₆ cluster has both extremely low first and second barriers (0.05 and 0.02 eV). Another crucial parameter is the total reaction energy E_r , which varies from -3.3 to -5.04 eV. The most energetically favorable path, on Cu₆Au₆, is ~ 1 eV lower than all the other ones. This higher gain in the energy comes from the rearrangement of metal atoms to a much more symmetric structure during stage R4.

The median activation barrier of the reaction is more than 3 times lower than the effective activation energy ~ 1.3 eV of the non-catalytic reaction.⁶³ We also compared our results with the corresponding values in the pure gold and copper clusters and surfaces.^{13,14,60,64,65} The results demonstrate that our values of limiting activation barriers are comparable with those in pure gold nanoclusters (~ 0.4 eV) and are lower than barriers in pure copper nanoclusters (~ 0.5 – 0.6 eV). Surfaces of bulk gold catalysts have lower barriers (~ 0.2 – 0.3 eV), but some of our clusters (Cu₇Au₆ *etc.*) have the lowest barriers. Structure reordering, which might occur during the reaction, may affect not only the reaction energy but also other aspects of the catalytic cycle. For example, in the CO oxidation on the Cu₃Au₅ cluster, rearrangement takes place during stage R4, causing migration of the O* atom from the copper to the gold atoms and thereby facilitating the subsequent recovery of the catalyst.

Some clusters considered in this study have more than one active site, and different reaction paths can be realized on one cluster. The prevailing path may depend on the environmental conditions, particularly the temperature. At lower temperatures, the system is likely to undergo the reaction with the lowest barrier. If the temperature is high enough to overcome the barriers, the preferred reaction is determined by the largest overall energy gain. A good example of such competition is the Cu₃Au₅ cluster, where for one reaction path, the overall energy decrease and the largest barrier are 3.4 and 0.32 eV, respectively, whereas for the other path, the corresponding values are 3.8 and 0.71 eV (cases 3 and 4 in Fig. 3). The first path has a lower barrier and the second one has a larger energy decrease. Similar behavior was also observed for Cu₄Au₆ and Cu₅Au₅ clusters. In some studies, in nanocatalysis the activation energy E_a and total reaction energy E_r are considered linearly dependent (relying on the Brønsted–Evans–Polanyi (BEP) statistical principle¹⁴); if a path has the lowest barrier, it should have the highest energy gain. The BEP prin-

ciple is known to be valid for reactions occurring on the same catalytic surface, but often applied to other systems like nanoclusters.¹⁴ In this study, an apparent violation of the BEP principle was observed for Cu–Au clusters, which we suggest can be due to a different nature of active sites at the cluster surface. One should also keep in mind that the BEP principle is valid only as a statistical trend and is often violated when looking at individual cases.

4. Conclusions

We performed a systematic study of CO oxidation on Cu–Au nanoclusters. First, the ground-state structures of Cu_{*n*}Au_{*m*} clusters were determined in a wide area of compositions ($n + m \leq 15$) using the USPEX method combined with density-functional theory calculations. On the basis of the energies of the optimal clusters, we assessed the local stability for each one through the minimum second derivative of their energy with respect to the number of atoms of each kind. To estimate potential catalytic activity, we found the lowest coordination number in all considered structures. Next, we selected nine promising candidates, which are suggested to be both stable and catalytically active and considered 18 different reactions of CO oxidation on these clusters. For each reaction, we calculated the adsorption energies of CO and O₂, energies of the transition states, and of the intermediates along the minimal energy pathway. We showed that the activation energies are often not higher than ~ 0.4 eV, which can be overcome under mild conditions, and thus it might be expected that most part of the experimentally synthesized ensemble of clusters would have high catalytic activity. In some cases, extremely low activation barriers (0.02–0.11 eV) were found, which can be due to the characteristic features of the reaction mechanisms; for example, the second barrier strongly depends on the coordination of an adsorbed O* atom when CO₂ is desorbed from a cluster. We also found an often-occurring structural rearrangement of clusters during the reaction, which can affect the energy gain and facilitate desorption of oxygen from the cluster. We showed that the activation energies of catalytic CO oxidation on Cu–Au clusters are equal to or lower than those in pure Au clusters. In addition to the lower cost of copper, this makes copper–gold clusters a new promising class of catalysts.

Author contributions

Anastasia A. Mikhailova; conceptualization, methodology, data curation, investigation, writing – original draft, writing – review and editing, and visualization. Sergey V. Lepeshkin; methodology, formal analysis, investigation, writing – original draft, and visualization. Vladimir S. Baturin; methodology, formal analysis, investigation, writing – original draft, and visualization. Alexey P. Maltsev; investigation, formal analysis, and writing – original draft. Yurii A. Uspenskii; conceptualiz-

ation and writing – review and editing. Artem R. Oganov; conceptualization, supervision, and writing – review and editing. All co-authors contributed to the discussion of the data. All authors have given approval to the final version of the manuscript.

Conflicts of interest

The authors declare no competing financial interest.

Acknowledgements

The calculation of the activation energies and pathways for CO oxidation was developed within the Project of the State Assignment (Vernadsky Institute of Geochemistry and Analytical Chemistry of the Russian Academy of Sciences, Moscow, Russian Federation). The calculations were performed on Oleg and Arkuda supercomputers at Skoltech, in the Joint Supercomputer Center of the Russian Academy of Sciences, and in Lobachevsky cluster at the University of Nizhny Novgorod. This work was supported by the Russian Science Foundation [grant number 19-72-30043].

References

- 1 M. Haruta, S. Tsubota, T. Kobayashi, H. Kageyama, M. J. Genet and B. Delmon, *J. Catal.*, 1993, **144**, 175–192.
- 2 M. Haruta, *Catal. Today*, 1997, **36**, 153–166.
- 3 M. Valden, X. Lai and D. W. Goodman, *Science*, 1998, **281**, 1647–1650.
- 4 G. R. Bamwenda, S. Tsubota, T. Nakamura and M. Haruta, *Catal. Lett.*, 1997, **44**, 83–87.
- 5 M. Haruta, *CATTECH*, 2002, **6**, 102–115.
- 6 I. X. Green, W. Tang, M. Neurock and J. T. Yates Jr., *Science*, 2011, **333**, 736–739.
- 7 R. Meyer, C. Lemire, S. K. Shaikhutdinov and H.-J. Freund, *Gold Bull.*, 2004, **37**, 72–124.
- 8 R. Ferrando, J. Jellinek and R. L. Johnston, *Chem. Rev.*, 2008, **108**, 845–910.
- 9 N. A. Gaya, V. Charles, I. Joseph and H. Louis, *Catal. Sustainable Energy*, 2019, **6**, 13–37.
- 10 N. Lopez and J. K. Nørskov, *J. Am. Chem. Soc.*, 2002, **124**, 11262–11263.
- 11 C. H. Christensen and J. K. Nørskov, *Science*, 2010, **327**, 278–279.
- 12 W. Zhan, J. Wang, H. Wang, J. Zhang, X. Liu, P. Zhang, M. Chi, Y. Guo, Y. Guo, G. Lu, S. Sun, S. Dai and H. Zhu, *J. Am. Chem. Soc.*, 2017, **139**, 8846–8854.
- 13 Y. Gao, N. Shao, Y. Pei, Z. Chen and X. C. Zeng, *ACS Nano*, 2011, **5**, 7818–7829.
- 14 H. Xu, D. Cheng, Y. Gao and X. C. Zeng, *ACS Catal.*, 2018, **8**, 9702–9710.
- 15 T. Bligaard, J. K. Nørskov, S. Dahl, J. Matthesen, C. H. Christensen and J. Sehested, *J. Catal.*, 2004, **224**, 206–217.
- 16 H. Falsig, B. Hvolbæk, I. S. Kristensen, T. Jiang, T. Bligaard, C. H. Christensen and J. K. Nørskov, *Angew. Chem.*, 2008, **120**, 4913–4917.
- 17 B. Hammer and J. K. Nørskov, *Nature*, 1995, **376**, 238–240.
- 18 J. A. van Bokhoven and J. T. Miller, *J. Phys. Chem. C*, 2007, **111**, 9245–9249.
- 19 B. Hvolbæk, T. V. W. Janssens, B. S. Clausen, H. Falsig, C. H. Christensen and J. K. Nørskov, *Nano Today*, 2007, **2**, 14–18.
- 20 J. J. Kim, D. P. Summers and K. W. Frese Jr., *J. Electroanal. Chem. Interfacial Electrochem.*, 1988, **245**, 223–244.
- 21 S. Pace, T. Van Hoof, M. Hou, C. Buess-Herman and F. Reniers, *Surf. Interface Anal.*, 2004, **36**, 1078–1082.
- 22 L. Wang and J. C. Yang, *J. Mater. Res.*, 2005, **20**, 1902–1909.
- 23 *Modern Aspects of Electrochemistry*, ed. C. G. Vayenas, R. E. White and M. E. Gamboa-Aldeco, Springer, New York, NY, 2008, vol. 42.
- 24 L. Delannoy, G. Thrimurthulu, P. S. Reddy, C. Méthivier, J. Nelayah, B. M. Reddy, C. Ricolleau and C. Louis, *Phys. Chem. Chem. Phys.*, 2014, **16**, 26514–26527.
- 25 Z. Xu, E. Lai, Y. Shao-Horn and K. Hamad-Schifferli, *Chem. Commun.*, 2012, **48**, 5626–5628.
- 26 S. Lysgaard, J. S. G. Mýrdal, H. A. Hansen and T. Vegge, *Phys. Chem. Chem. Phys.*, 2015, **17**, 28270–28276.
- 27 Y.-C. Lu, Z. Xu, H. A. Gasteiger, S. Chen, K. Hamad-Schifferli and Y. Shao-Horn, *J. Am. Chem. Soc.*, 2010, **132**, 12170–12171.
- 28 J. Monzó, Y. Malewski, R. Kortlever, F. J. Vidal-Iglesias, J. Solla-Gullón, M. T. M. Koper and P. Rodriguez, *J. Mater. Chem. A*, 2015, **3**, 23690–23698.
- 29 K. Koga and D. Zubia, *J. Phys. Chem. C*, 2008, **112**, 2079–2085.
- 30 S. Darby, T. V. Mortimer-Jones, R. L. Johnston and C. Roberts, *J. Chem. Phys.*, 2002, **116**, 1536–1550.
- 31 R. Du, S. Tang, X. Wu, Y. Xu, R. Chen and T. Liu, *R. Soc. Open Sci.*, 2016, **6**(8), 190342.
- 32 I. V. Chepkasov, V. S. Baidyshev, A. A. Golubnichiy, I. S. Zamulin, A. G. Kvashnin and S. M. Kozlov, *Aggregate*, 2022, **3**, 6.
- 33 J. R. H. Ross, *Heterogeneous Catalysis: Fundamentals and Applications*, Elsevier, 2011.
- 34 J.-X. Liu, I. A. W. Filot, Y. Su, B. Zijlstra and E. J. M. Hensen, *J. Phys. Chem. C*, 2018, **122**, 8327–8340.
- 35 P. Rodriguez, D. Plana, D. J. Fermin and M. T. M. Koper, *J. Catal.*, 2014, **311**, 182–189.
- 36 H. Lee, J. Lim, C. Lee, S. Back, K. An, J. W. Shin, R. Ryoo, Y. Jung and J. Y. Park, *Nat. Commun.*, 2018, **9**, 2235.
- 37 X. Liao, Y. Liu, W. Chu, S. Sall, C. Petit, V. Pitchon and V. Caps, *J. Catal.*, 2020, **382**, 329–338.
- 38 T.-S. Kim, H. Choi, D. Kim, H. C. Song, Y. Oh, B. Jeong, J. Lee, K.-J. Kim, J. W. Shin, H. R. Byon, R. Ryoo, H. Y. Kim and J. Y. Park, *Appl. Catal., B*, 2023, **331**, 122704.

- 39 S. V. Lepeshkin, V. S. Baturin, Y. A. Uspenskii and A. R. Oganov, *J. Phys. Chem. Lett.*, 2019, **10**, 102–106.
- 40 A. R. Oganov and C. W. Glass, *J. Chem. Phys.*, 2006, **124**, 244704.
- 41 A. O. Lyakhov, A. R. Oganov, H. T. Stokes and Q. Zhu, *Comput. Phys. Commun.*, 2013, **184**, 1172–1182.
- 42 N. Bushlanova, V. Baturin, S. Lepeshkin and Y. Uspenskii, *Nanoscale*, 2021, **13**, 19181–19189.
- 43 V. Baturin, S. Lepeshkin, N. Bushlanova and Y. Uspenskii, *Phys. Chem. Chem. Phys.*, 2020, **22**, 26299–26305.
- 44 R. P. Gupta, *Phys. Rev. B: Condens. Matter Mater. Phys.*, 1981, **23**, 6265–6270.
- 45 S. Plimpton, *J. Comput. Phys.*, 1995, **117**, 1–19.
- 46 P. E. Blöchl, *Phys. Rev. B: Condens. Matter Mater. Phys.*, 1994, **50**, 17953–17979.
- 47 J. P. Perdew, K. Burke and M. Ernzerhof, *Phys. Rev. Lett.*, 1996, **77**, 3865–3868.
- 48 G. Kresse and J. Furthmüller, *Phys. Rev. B: Condens. Matter Mater. Phys.*, 1996, **54**, 11169–11186.
- 49 G. Kresse and J. Hafner, *Phys. Rev. B: Condens. Matter Mater. Phys.*, 1993, **47**, 558–561.
- 50 A. Tkatchenko and M. Scheffler, *Phys. Rev. Lett.*, 2009, **102**, 073005.
- 51 P. Lindgren, G. Kastlunger and A. A. Peterson, *J. Chem. Theory Comput.*, 2019, **15**, 5787–5793.
- 52 G. Henkelman and H. Jónsson, *J. Chem. Phys.*, 2000, **113**, 9978–9985.
- 53 H. A. Hussein, M. Gao, Y. Hou, S. L. Horswell and R. L. Johnston, *Z. Phys. Chem.*, 2019, **233**, 813–843.
- 54 C. J. Heard and R. L. Johnston, *Eur. Phys. J. D*, 2013, **67**, 34.
- 55 E. M. Fernández, L. C. Balbás, L. A. Pérez, K. Michaelian and I. L. Garzón, *Int. J. Mod. Phys. B*, 2005, **19**, 2339–2344.
- 56 P. Ranjan, T. Chakraborty and A. Kumar, *Chem. Nanosci. Nanotechnol.*, 2019, 33–42.
- 57 A. Chmielewski, J. Nelayah, H. Amara, J. Creuze, D. Alloyeau, G. Wang and C. Ricolleau, *Phys. Rev. Lett.*, 2018, **120**, 025901.
- 58 E. K. Rideal, *Nature*, 1940, **146**, 603–604.
- 59 D. D. Eley and E. K. Rideal, *Nature*, 1940, **146**, 401–402.
- 60 D. Tang and J. Zhang, *RSC Adv.*, 2013, **3**, 15225.
- 61 L. Ma and J. Akola, *Phys. Chem. Chem. Phys.*, 2019, **21**, 11351–11358.
- 62 S. Kozuch and S. Shaik, *Acc. Chem. Res.*, 2011, **44**, 101–110.
- 63 H. K. D. Hsuen and S. V. Sotirchos, *Chem. Eng. Sci.*, 1989, **44**, 2653–2665.
- 64 Y. Wang, G. Wu, M. Yang and J. Wang, *J. Phys. Chem. C*, 2013, **117**, 8767–8773.
- 65 L. Ma, M. Melander, K. Laasonen and J. Akola, *Phys. Chem. Chem. Phys.*, 2015, **17**, 7067–7076.